

# Mesososcopic simulations of phase distribution effects on the effective thermal conductivity of microgranular porous media

Moran Wang<sup>a,\*</sup>, Ning Pan<sup>a</sup>, Jinku Wang<sup>b</sup>, Shiyi Chen<sup>c</sup>

<sup>a</sup> Department of Biological and Agricultural Engineering, University of California, Davis, CA 95616, USA

<sup>b</sup> School of Aerospace, Tsinghua University, Beijing 100084, China

<sup>c</sup> Department of Mechanical Engineering, The Johns Hopkins University, Baltimore, MD 21218, USA

Received 31 October 2006; accepted 20 March 2007

Available online 24 March 2007

## Abstract

This paper analyzes the phase distribution effects on the effective thermal conductivity (ETC) of multi-phase microgranular porous media using mesoscopic statistics based numerical methods. A multi-parameter random generation-growth method, quartet structure generation set (QSGS), is developed for replicating microstructures of multi-phase granular porous media based on the macroscopic statistical information, such as the volume fractions and the phase interactions. The phase distribution characteristics and the interphase connections are controlled by adjusting the related parameters. Then the energy transport equations through porous media are solved by a lattice Boltzmann method developed by us with multi-phase conjugate heat transfer considered. The results indicate that a smaller average particle size could lead to a larger effective thermal conductivity of two-phase porous media for a certain porosity. For the anisotropic media, if the larger directional growth probability is along the direction of temperature gradient, the effective thermal conductivity in the parallel direction is enhanced as a result, and that in the vertical direction will be weakened. For multi-phase porous media, the degree of phase conglomeration is determined by the phase interactions. A larger liquid–liquid interaction leads to a higher degree of liquid phase conglomeration and therefore a larger effective thermal conductivity of the porous media.

© 2007 Elsevier Inc. All rights reserved.

**Keywords:** Effective thermal conductivity; Microporous media; Phase distribution; Anisotropy

## 1. Introduction

The thermal properties of porous media have been of great interests recently due to their applications in science and engineering, such as material design, geophysical exploration, biological and medical engineering [1–8]. Most previous theoretical models for predicting the effective thermal conductivities (ETC) are based on the network combinations of Series and Parallel models [9–12] or on the uniform phase assumption [12]. Although these models are easy to use because of their simple dependence on phase fractions, the effects of phase distribution and multi-phase interaction on the effective thermal conductivities are yet ignored. A full numerical determination of thermal properties of porous media generally includes two

steps: Acquiring the structure and phase distribution information into consideration and then solving the relevant set of local energy transport equations.

Several methods have been proposed to generate microstructures of multi-phase materials in the past decade. Tacher et al. [13] presented a discrete reduced distance method to generate spherical/elliptical two-phase granular porous media. Based on Tacher's work, Pilotti developed a grains sedimentation algorithm [14]. Both Tacher's and Pilotti's methods generate porous media with random size and locations, however, neither can deal well with the connections between grains. Therefore neither is suitable for the heat transfer problems which are extremely sensitive to connections. Recently, the reconstruction process has been widely used in generating random two-phase [15,16] and multi-component [17,18] porous materials based on the digital microtomographic information and statistical correlation functions [19]. This kind of reconstruction method is

\* Corresponding author.

E-mail address: [mmwang@ucdavis.edu](mailto:mmwang@ucdavis.edu) (M. Wang).

more suitable for non-fluidic or single-fluid systems but not for multiple fluid systems. Mohanty [20] therefore generated unsaturated porous media using a Monte Carlo annealing algorithm based on the law of lowest interfacial energy. However, one can notice from the available data and images that the lowest-energy law is, but not always, the rule dominating the phase distributions of porous media where random factors may play more important roles, especially in micro porous media [18]. Wang et al. [21,22] proposed a multi-parameter random generation-growth method, termed quartet structure generation set (QSGS), to replicate randomly distributed multi-phase granular porous media based on the cluster growth theory [7, 23] and then investigated the thermal conductivity of isotropic porous media.

To solve the relevant set of local energy transport equations, the traditional partial differential equation (PDE) solvers, such as finite difference method (FDM) and finite element method (FEM), have been applied for the first steps [24–26]. However, such traditional PDE solvers demand huge or often unacceptable computational resources when the porous structure becomes complicated, especially when the fluid–solid conjugate heat transfer problem is considered [27,28]. Meanwhile the stochastic methods for representing the perturbations in porous media have gained much attention recently [29,30]. Shoshany et al. [31] and Barta and Dieska [32] modeled the thermal conductivity of porous materials using the Monte Carlo methods to reflect the structural fluctuations during the process. Zhang et al. [33,34] developed a randomly mixed material model (RMM) for predicting the effective thermal conductivity of moist porous media. Qian et al. [35] proposed a two-dimensional five-speed (D2Q5) lattice Boltzmann model to simulate the effective thermal conductivity of porous media, while neglecting the solid–fluid conjugate heat transfer, which actually plays a critical role in thermal transport in porous media [36,37].

Following our previous work, we develop the QSGS further for generating microstructures of multi-phase porous media with emphasis on the parameter effects on phase distributions. After the microstructures of porous media are generated, the thermal conduction equations are solved by a lattice Boltzmann method with multi-phase conjugate heat transfer effects considered. The phase distribution effects on the ETC of microgranular porous media are thus analyzed.

## 2. Numerical methods

### 2.1. Randomly generation-growth algorithm for generating porous structures

Before the generation, one needs to determine which phase is the non-growing phase and then the rests are growing phases. In the present paper, we call the non-growing phase the first phase, and the growing phase as the  $n$ th phase, where  $n = 2$  to  $N$ , the total number of phases in the system. Without losing generality, the discrete phases are normally taken as the growing phases. For example, rocks and water are the grow-

ing phases in unsaturated sands, while the gas is the growing phase for the polyurethane foams.

The QSGS for generating porous structures includes six steps [21]:

- (i) Randomly locate the cores of the first growing phase in a grid system based on a core distribution probability,  $c_d$ , whose value is no greater than the volume fraction of the phase. Each cell in the grid will be assigned a random number by a uniform distribution function within (0, 1). Each cell whose random number is no greater than  $c_d$  will be chosen as a core.
- (ii) Enlarge every element of the growing phase to its neighboring cells in all directions based on each given directional growth probability,  $D_i$ , where  $i$  represents the direction. Again for each growing element, new random numbers will be assigned to its neighboring cells. The neighboring cell in direction  $i$  will become part of the growing phase if its random number is no greater than  $D_i$ .
- (iii) Repeat the growing process of (ii) until the volume fraction of the first growing phase reaches its given value  $P^2$  (if the growing phase is gas,  $P^2$  is more often expressed as the porosity  $\varepsilon$ ).
- (iv) As to the next growing phase, there are two cases to consider depending on its interaction with the existing phase(s). If this phase is an equivalent discrete phase as the existing growing phase, such as multi-component mixture, it grows from separate seeds, which is very similar as the first growing phase described in (i–iii). Otherwise, we have to consider the constraint by and interaction with the existing phase(s). For such cases, the  $n$ th phase ( $n > 2$ ) will grow based on a phase interaction growth probability,  $I_i^{n,m}$ , which represents the growth probability of the  $n$ th phase on the  $m$ th phase along the  $i$ th direction;
- (v) Stop the  $n$ th phase growth once its volume fraction reaches the given value  $P^n$ .
- (vi) Repeat the next phase growth as described in (iv) and (v) until  $n = N$ . The spaces not occupied at the end represent the non-growing phase.

Thus, there are four parameters ( $c_d$ ,  $D_i$ ,  $P^n$ ,  $I_i^{n,m}$ ) controlling the microstructures of generated porous media based on the generation process. The core distribution probability  $c_d$  is defined as the probability of a cell to become a core of the first growing phase on which growth or expansion of the first phase originates. The value of  $c_d$  indicates the number density of growing cores for the first growing phase, to reflect the statistical distribution of the first growing phase throughout the system. The  $c_d$  value thus also controls the degree of structure details of a system; a smaller  $c_d$  leads to a finer description of the microstructures including particle/pore shapes and inter-particle/pore connections, etc. However a small  $c_d$  value will also decrease the statistical particle numbers for a given grid size and thus increase the computation fluctuation.

The directional growth probability  $D_i$  is defined as the probability for a yet to be occupied cell to merge into a neighboring cell in the  $i$ th direction to become part of the growing phase. An

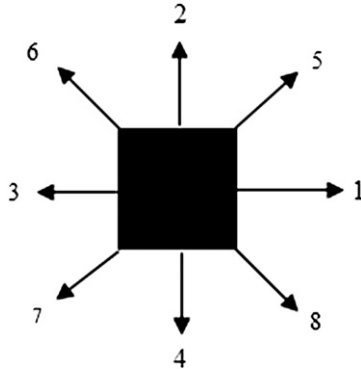


Fig. 1. Eight growth directions of each point for 2D systems.

appropriate arrangement of the directional growth probabilities may lead to an isotropic structure. In other words, the growth probabilities can be adjusted to control the degree of anisotropy. For two-dimensional cases, each square cell has eight growing directions to its neighbors, as seen in Fig. 1. There are four main directions (1, 2, 3, 4) and four diagonal directions (5, 6, 7, 8). To obtain an isotropic structure in such systems, we set both the main directional growth probabilities  $D_{1-4}$  and the diagonal directional growth probabilities  $D_{5-8}$  into respective constant in each group, and the both constants in a fixed ratio. For instance, by designating the probabilities ratio,  $D_{1-4}:D_{5-8} = 4$ , we get the directional growth probability consistent with the equilibrium density distribution function for isotropic materials [38,39].

For multi-phase porous media systems ( $n > 2$ ), the interactions between different discrete phases become even more complex, and we have to consider the effects of such interactions during the phase growth. Such effects are important especially, for instance, in unsaturated porous media soaked by a liquid that wets other phases in the system differently. In such systems, the growth order of the various phases is important. Generally the solid phase is selected as the first growing phase and then the liquid phase grows under the influences of phase interactions. The phase interaction growth probability,  $I_i^{n,m}$ , i.e., the growth probability of  $n$ th phase on the surface of  $m$ th phase along the  $i$ th direction, is hence introduced to account for this influence by assigning different values to  $I_i^{n,m}$  for different materials. The value of the phase interaction growth probability  $I_i^{n,m}$  could be determined by analyzing the scanned pictures of phase distributions or by calculating from the wetting properties directly.

Comparing with the existing generation methods, the QSGS may have following merits: (i) The generation-growth process is very close to the natural formation process of most real porous media which grow outward from cores. Therefore the generated microstructure is more realistic. (ii) Each of the parameters in the algorithm has a distinct physical significance, instead of an empirical determination. (iii) It deals well with multi-body connection problems. (iv) The stochastic and statistical features of system are determined before the treatment by the physical laws, instead of other way around as in many existing methods, thus facilitating smoother tackling of the physical problems in a more realistic setting (the material is already there before modeling). (v) The method is efficient without turning to

any iteration process. The algorithm is straightforward in three-dimensional and/or multi-phase cases, and suitable for parallel computing.

## 2.2. Lattice Boltzmann algorithm for solving energy equations

The lattice Boltzmann method (LBM) is intrinsically a mesoscopic approach based on the evolution of statistical distribution on lattices, and has achieved considerable success in simulating fluid flows and associated transport phenomena [40–43]. The most important advantages of the LBM are the easy implementations of multiple inter-particle interactions and complex geometry boundary conditions [44–46], and the conservation laws can hold automatically in general without additional computational efforts [47]. The LBM thermal models have been developed recently [48,49]. Here we introduce our previous lattice Boltzmann algorithm for fluid–solid conjugate heat transfer [37], and adapt it for effective thermal conductivity predictions.

For a pure thermal conduction in porous media with no phase change, no heat source and no convection, the temperature evolution equation for each phase is generally written as

$$g_\alpha(\mathbf{r} + \mathbf{e}_\alpha \delta_t, t + \delta_t) - g_\alpha(\mathbf{r}, t) = -\frac{1}{\tau_n} [g_\alpha(\mathbf{r}, t) - g_\alpha^{\text{eq}}(\mathbf{r}, t)], \quad (1)$$

which is actually a simplified form for multi-phase conjugate heat transfer by eliminating the convection and heat source terms [37]. The equilibrium distribution of the evolution variable,  $g_\alpha$ , for the two-dimensional nine-speed (D2Q9) model is

$$g_\alpha^{\text{eq}} = \begin{cases} 0, & \alpha = 0, \\ T/6, & \alpha = 1, 2, 3, 4, \\ T/12, & \alpha = 5, 6, 7, 8, \end{cases} \quad (2)$$

the microscopic velocity

$$\mathbf{e}_\alpha = \begin{cases} (0, 0), & \alpha = 0, \\ (\cos \theta_\alpha, \sin \theta_\alpha) c, & \alpha = 1, 2, 3, 4, \\ \sqrt{2}(\cos \theta_\alpha, \sin \theta_\alpha) c, & \alpha = 5, 6, 7, 8, \end{cases} \quad (3)$$

and the dimensionless relaxation time

$$\tau_n = \frac{3}{2} \frac{k_n}{(\rho c_p)_n c^2 \delta_t} + 0.5, \quad (4)$$

where the subscript  $n$  still represents the  $n$ th phase,  $\delta_t$  the time step,  $k$  the thermal conductivity, and  $c$  a *pseudo* sound speed whose value can take any positive value theoretically only to insure  $\tau$  values within (0.5, 2) [42]. To meet the requirement of temperature and heat flux continuities at phase interfaces, we have to assume identical volume thermal capacities  $(\rho c_p)$  for different phases; the conjugate heat problem between different phases is thus solved and these assumptions will not affect the effective thermal conductivity calculated [36]. The temperature and the heat flux are then calculated by

$$T = \sum_{\alpha} g_\alpha, \quad (5)$$

$$q = \left( \sum_{\alpha} \mathbf{e}_{\alpha} g_{\alpha} \right) \frac{\tau_n - 0.5}{\tau_n}. \quad (6)$$

For the isothermal boundary treatment, we follow the bounce-back rule of the non-equilibrium distribution proposed by Zou and He [50]:

$$g_{\alpha} - g_{\alpha}^{\text{eq}} = -(g_{\beta} - g_{\beta}^{\text{eq}}), \quad (7)$$

where the subscripts  $\alpha$  and  $\beta$  represent two opposite directions respectively, and the equilibrium distribution can be calculated using the local boundary temperatures.

For the insulated boundary, we have tried the Neumann boundary treatment [37] and let the boundary temperature gradient equal to zero. However heat flux leak will result along the insulated surfaces. Therefore a specular reflection boundary condition is implemented here

$$g_{\alpha} = g_{\beta}. \quad (8)$$

After the temperature field is solved, the ETC,  $k_{\text{eff}}$ , can finally be determined as

$$k_{\text{eff}} = \frac{L \int q \, dA}{\Delta T \int dA}, \quad (9)$$

where  $q$  is the steady heat flux through the media cross-section area  $dA$  between the temperature difference  $\Delta T$  with a distance  $L$ .

### 3. Validations

To validate the present methods for calculating the effective thermal conductivity of micro porous media, this section compares the numerical results with the existing theoretical solutions and experimental data.

#### 3.1. Theoretical solutions

First we validate the numerical solver by calculating the effective thermal conductivities for two basic structures of double-component materials: the Parallel mode and the Series mode (see Fig. 2). Assuming the thermal conductivity of each

component is  $k_1$  and  $k_2$ , respectively, the simple theoretical solutions give the effective thermal conductivities as  $(k_1 + k_2)/2$  for the Parallel mode and  $1/(1/2k_1 + 1/2k_2)$  for the Series mode.

Table 1 lists the calculated effective thermal conductivities comparing with theoretical solutions for different values of  $k_2$ ,  $k_1$  is kept constant as 1.0 W/m K while  $k_2$  changes from 2.0 to 1000 W/m K. The results show the deviations are no greater than 0.02% for the Parallel mode and 0.25% for the Series mode, which indicates good accuracy of the present numerical solver.

#### 3.2. Experimental data

Second we combine the QSGS for generating random multi-phase structure with the LBM solver for solving the energy transport equations together, and then predict the effective thermal conductivity of heterogeneous materials. The numerical results are compared with two experimental cases.

Consider a two-phase composite, Cu/solder where the Cu particles are uniformly dispersed in the solder mass. The solder is selected as the non-growing (first) phase and the Cu particles are the growing (second) phase. The component thermal conductivities are  $k_{\text{Cu}} = 398.0$  W/m K and  $k_{\text{solder}} = 78.1$  W/m K. Fig. 3 shows the predicted effective thermal conductivities as a function of Cu volume fraction,  $P_2(\varepsilon)$ , which are compared

Table 1

$k_1:k_2$	Mode	Theoretical value (W/m K)	Numerical value (W/m K)	Deviation (%)
1:2	Parallel	1.500	1.500	0.000
	Series	1.333	1.332	0.075
1:10	Parallel	5.500	5.500	0.000
	Series	1.818	1.814	0.220
1:100	Parallel	50.50	50.50	0.000
	Series	1.980	1.975	0.250
1:500	Parallel	250.5	250.5	0.000
	Series	1.996	1.991	0.250
1:1000	Parallel	500.5	500.4	0.020
	Series	1.998	1.993	0.250

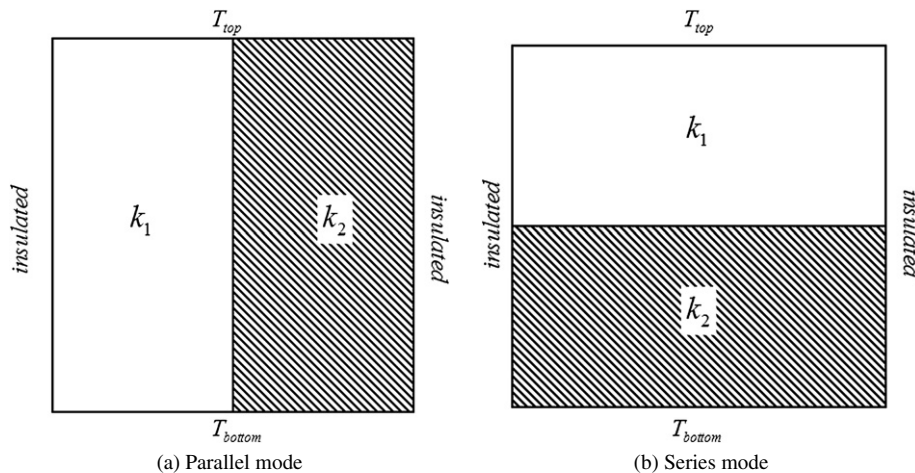


Fig. 2. Two basic structures for validation.



with the experimental data from [51]. The phase distribution details are unknown so that we have to make common-sense estimates. The parameters used in present QSGS are  $c_d = 0.01$  and  $D_{1-4}:D_{5-8} = 4:1$ . The numerical results agree with the experimental data pretty well.

The unsaturated porous media are then studied which involve three phases in one system. Customarily, the porosity,  $\varepsilon$ , is defined as the total volume fraction of the fluids. The degree of saturation,  $S$ , is defined as the liquid volume fraction within the fluids. Therefore the solid phase, the liquid phase, and the gas phase have the volume fractions of  $(1 - \varepsilon)$ ,  $\varepsilon S$ , and  $\varepsilon(1 - S)$ , respectively. Fig. 4 shows the predicted effective thermal conductivities versus the degree of saturation  $S$  for moist porous brick sands in both frozen and unfrozen states. The numerical results are compared again with the experimental data [52,53]. The QSGS parameters are  $c_d = 0.01$ ,  $D_{1-4}:D_{5-8} = 4:1$ ,  $\varepsilon = 0.52$  and  $I_i^{3,2} = I_i^{3,3}$  for each  $i$  direction. The thermal conductivities used in the simulations are,

$k_s = 2.85$  W/m K,  $k_w = 0.5924$  W/m K,  $k_g = 0.0249$  W/m K, and  $k_{ice} = 2.38$  W/m K [53,54]. A  $200 \times 200$  grid is used in the simulations, yielding the random fluctuation within 3%. Once again, good agreements are obtained with the experimental data for both frozen and unfrozen cases.

#### 4. Results and discussion

This section will focus on the phase distribution effects on the effective thermal conductivity of microgranular porous media by changing parameter values for the microstructure. Recently the three-dimensional effects have been analyzed on the ETC of granular porous media and it was found that most experimental data measured by the hot probe and the hot agreed with the two-dimensional predictions [22]. Since the hot probe and the hot wire are still most popular measurement methods for the ETC of granular porous media, our simulations in the present work focus on two-dimensional cases.

##### 4.1. Pore/particle size effects

Several researchers have reported that the effective thermal conductivities of porous media may differ for different average pore/particle sizes by their experiments even though the components and the porosities of the media are same [55–58]. For the solid–air porous system, a finer solid particles medium often led to a higher effective thermal conductivity at a same porosity [57,58]. This phenomenon can hardly be explained by the existing theoretical model for ETC, and few analyses have been found to focus on the mechanism so far.

Here we control the average pore/particle size by changing the values of  $c_d$ . A greater value of  $c_d$  leads to a smaller average size of pores/particles for a certain porosity  $\varepsilon$ . Fig. 5 demonstrates two generated structures at  $\varepsilon = 0.5$  where (a) has a ten times higher  $c_d$  than (b) does. The structure for a higher  $c_d$  looks more uniform and has a higher surface-to-volume ratio. The noisy surfaces of the generated structure could be regarded as a typical feature of natural granular porous media. The therefore complexities of structure may increase greatly computational costs of any classical PDE solvers, however, do not affect the computational efficiency of the LBM calculations much.

After the porous structures are generated for different values of  $c_d$ , the particle size effect on ETC of porous media is then investigated. Fig. 6 shows the predicted ETC versus solid volume fraction  $(1 - \varepsilon)$  for two different values of  $c_d$ . The thermal conductivities of the components are  $k_s = 3.0$  W/m K and  $k_g = 0.025$  W/m K. The theoretical solutions for Parallel mode and Series mode are also compared in the same figure. The results show that the ETC's of random porous media are between the values of Parallel mode and Series mode, and a larger average particle size leads to a lower ETC of porous media for all range of porosity except 0 and 1. The largest difference between ETCs for different values of  $c_d$  occurs when the solid volume fraction is within 0.5–0.8. Thus we keep the solid volume fraction at 0.5 and change the value of  $c_d$ . The predicted ETCs for different values of  $c_d$  are then shown in Fig. 7, which indicates the ETC value increases with the core distribution possibility.

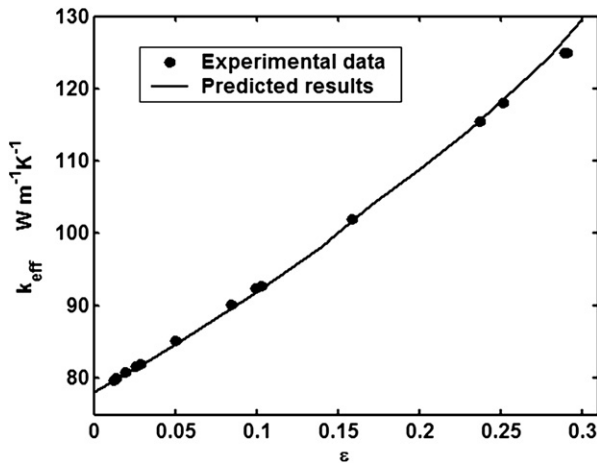


Fig. 3. Comparisons between predictions and experimental data for Cu/solder material. The experimental data is from Ref. [51]. The parameters are  $k_{Cu} = 398.0$  W/m K and  $k_{solder} = 78.1$  W/m K.

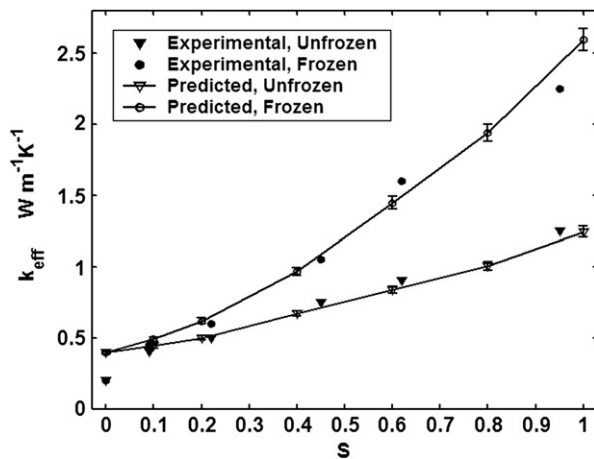


Fig. 4. Comparisons between predicted and experimental effective thermal conductivities of unsaturated porous sands in frozen and unfrozen states. The experimental data is from Refs. [52,53]. The parameters are  $\varepsilon = 0.52$ ,  $k_s = 2.85$  W/m K,  $k_w = 0.5924$  W/m K,  $k_g = 0.0249$  W/m K, and  $k_{ice} = 2.38$  W/m K.

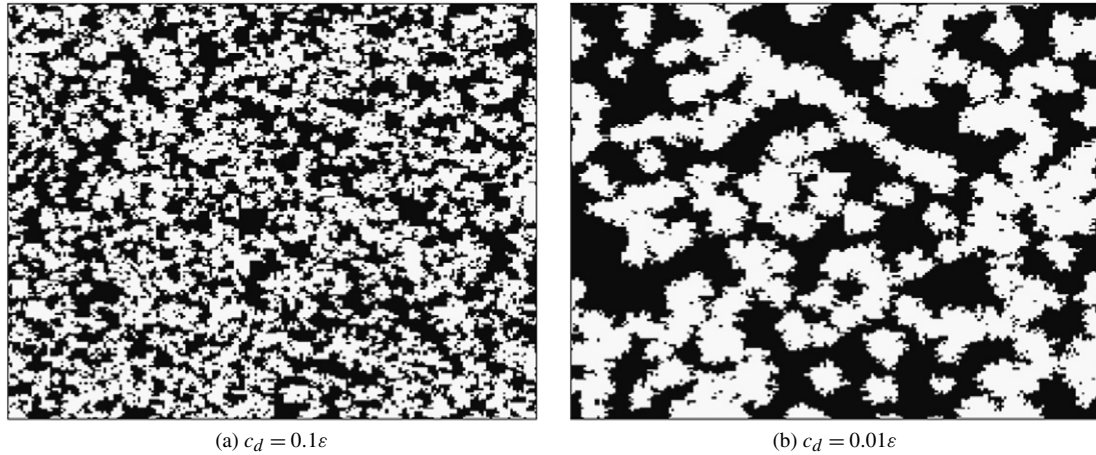


Fig. 5. Structures for different values of  $c_d$  at a same porosity  $\varepsilon = 0.5$ . The directional parameters are set as  $D_{1-4}:D_{5-8} = 4:1$ . The dark is gas and the white is solid.

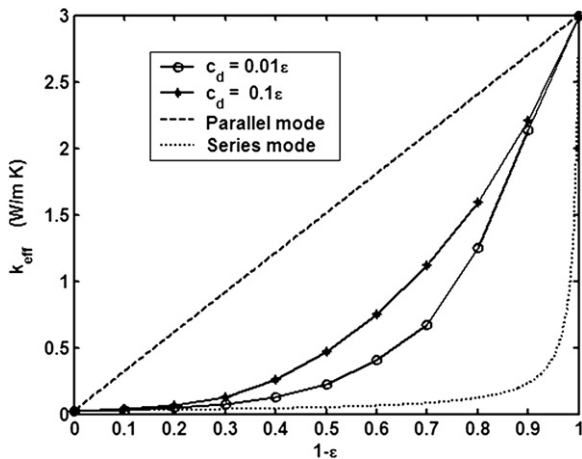


Fig. 6. ETC versus solid volume fraction for different values of  $c_d$ .

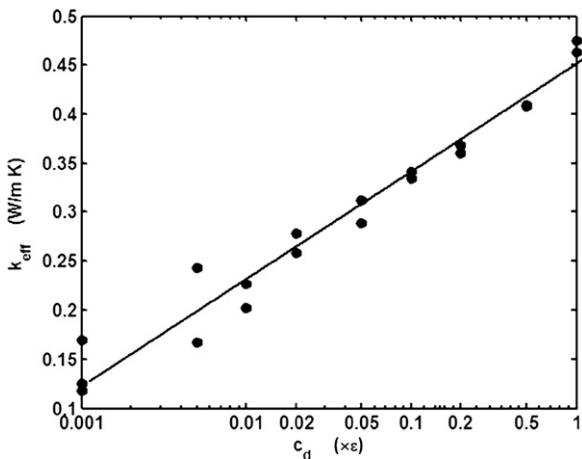


Fig. 7. ETC versus value of  $c_d$  at  $\varepsilon = 0.5$ .

Since the particle average volume is inversely proportional to the value of  $c_d$ , the result means the ETC of porous media decreases monotonically with the particle average size.

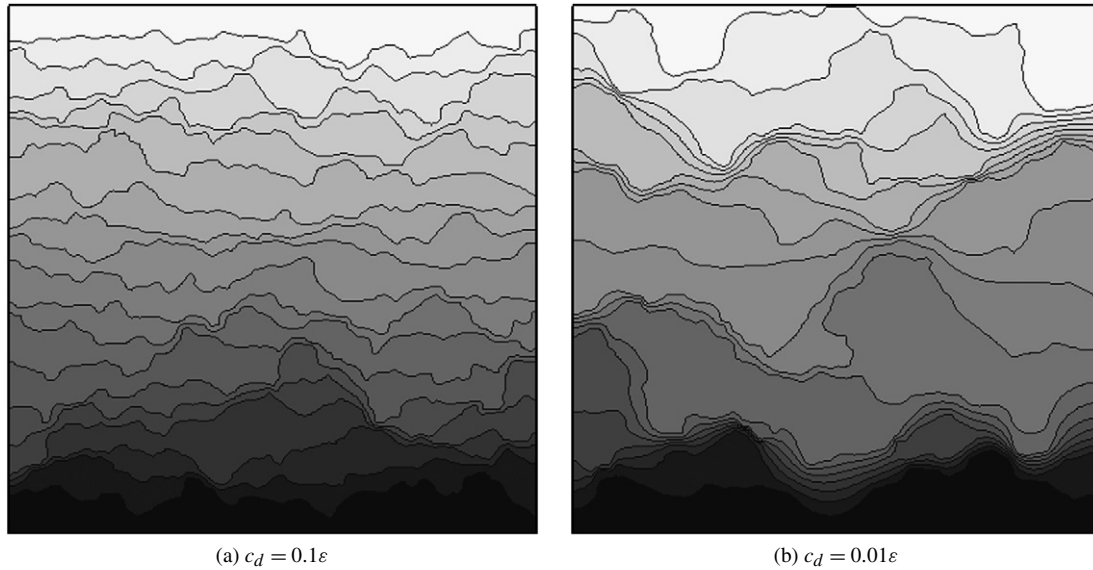
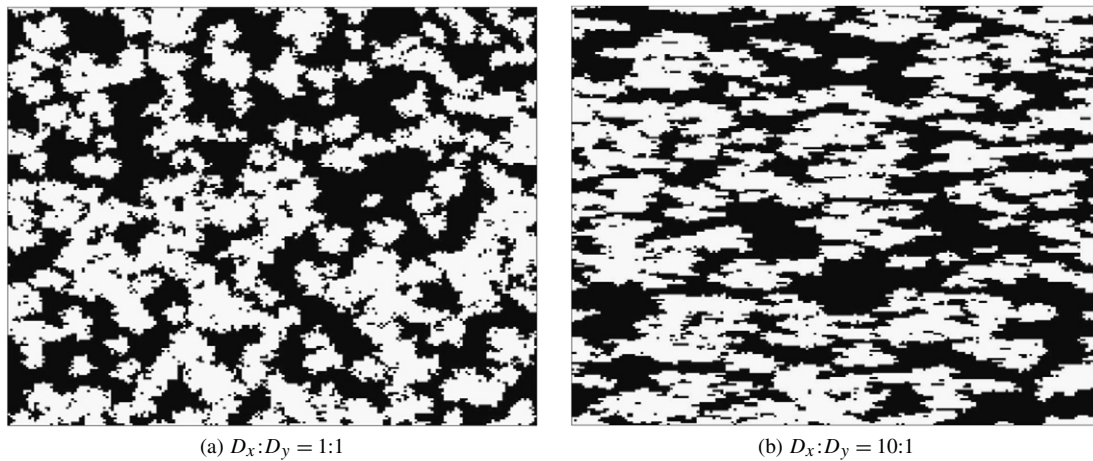
To discuss the mechanism why a smaller average particle size leads to a higher ETC of porous media, we give the temperature fields for different structures in Fig. 8. The top and

bottom boundaries are isothermal so that the temperature contours should be a series of uniform parallel lines for a homogeneous material. The temperature contours in the porous materials have been disturbed by the heterogeneous phase distributions, as shown in Fig. 8. However we still find that a larger value of  $c_d$  results in smoother temperature contours which are closer to those for homogeneous materials. Based on the uniformity principle of temperature gradient [59], the porous structure generated by a larger value of  $c_d$  deserves a higher ETC.

#### 4.2. Anisotropy effects

Most previous work has focused on the isotropic porous media. A few researchers generated anisotropic porous material by ellipse groups with different axis length or orientation angles [13]. Here we can achieve anisotropic phase distributions easily based on the QSGS process by varying values of the directional growth probability,  $D_i$ . No additional efforts are needed to deal with the inter-particle connections. Fig. 9 shows the generated structures for different ratio values of  $D_x:D_y$ , where  $D_x$  is the horizontal main directions (directions 1 and 3 in Fig. 1) and  $D_y$  is the vertical main directions (directions 2 and 4 in Fig. 1). The growth probabilities in the four diagonal directions are always set as a quarter of minimum of those in the main directions. The other parameters are  $c_d = 0.01$ ,  $\varepsilon = 0.5$  and the grid used is  $200 \times 200$ . The generated microstructures show quite different characteristics for different values of directional growth probabilities. The anisotropy increases with the  $D_x:D_y$  ratio. The directional growth probability corresponds to the macro structure statistical information, and can thus be determined by the measurement data from real porous structures.

After the anisotropic microstructures are generated, we change the  $D_x:D_y$  ratio from 0.01 to 100 and predict the effective thermal conductivity along the y direction. Fig. 10 shows the numerical results where  $\varepsilon = 0.5$ ,  $c_d = 0.01\varepsilon$ ,  $k_s = 3.0$  W/mK, and  $k_g = 0.025$  W/mK. The results indicate that the effective thermal conductivities along the y direction decrease monotonically with the  $D_x:D_y$  ratio. For a given porosity, the effective thermal conductivity is enhanced along the

Fig. 8. Temperature contours for different values of  $c_d$ .Fig. 9. Microstructures of anisotropic porous media with different directional growth probabilities with  $c_d = 0.01$ ,  $\varepsilon = 0.5$ . The dark is gas and the white is solid.

direction with higher growth probability and meanwhile weakened along the direction with lower growth probability.

#### 4.3. Phase interaction effects

When a porous medium contains more than two phases, usually the multi-phase interaction effects on the material properties have to be considered. For a three-phase porous system involving gas, liquid and solid, the simplest case is to generate the liquid phase with a uniform phase interaction growth probability, i.e.,  $I_i^{l,l}:I_i^{l,s} = 1$  with  $l$  representing the liquid phase and  $s$  the solid phase. This hypothesis is based on a strong wetting effect caused by a strong liquid–solid attractive potential, and will result in a uniform liquid film attached on the solid grains as shown in Fig. 11a. The smaller is the  $I_i^{l,l}:I_i^{l,s}$  ratio, the more uniform is the liquid film (see Fig. 11b). Such structures can be found in some multi-components composite materials [17]. However for the unsaturated sandstones or glass assemblies, the wetting characteristic of water may be different. Both the lowest interface energy law [20] and the measured images [60] have

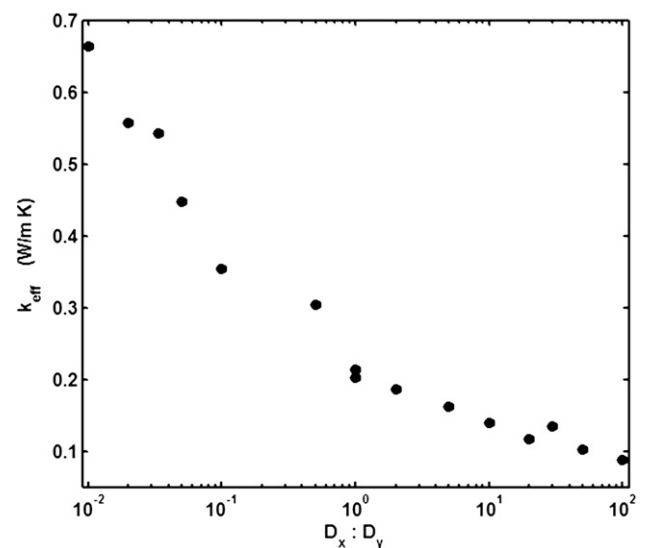


Fig. 10. ETC of anisotropic porous media for different directional growth probabilities.



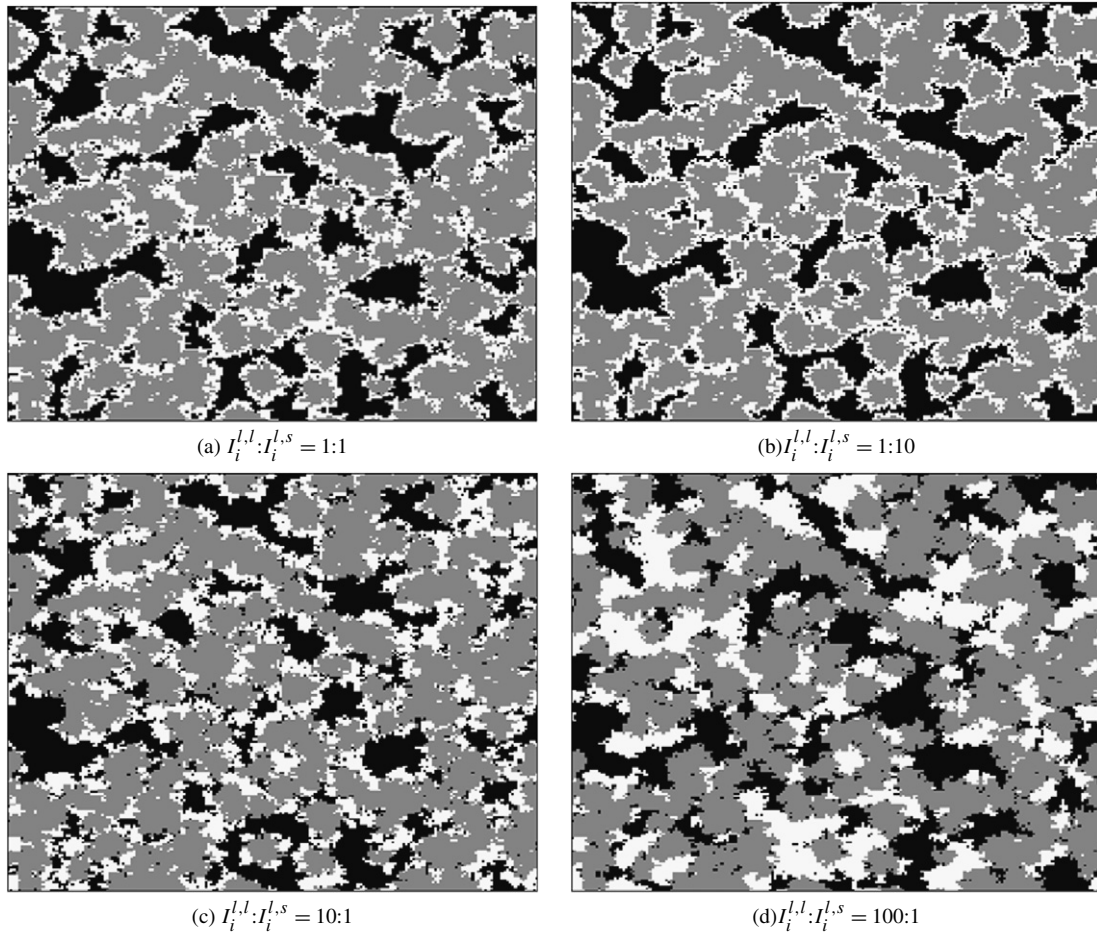


Fig. 11. Microstructures of three-phase porous media with different phase interaction growth probabilities. The gray is solid particles, the white is liquid, and the dark is gas. The solid is isotropic with  $c_d = 0.01\varepsilon$ . The porosity  $\varepsilon(P_2) = 0.5$ , and the liquid volume fraction  $P_l = 0.25$ .

shown that the water in sandstones or glass assemblies tends to be in conglomeration rather than in films on the solid surfaces due to the weak wetting properties. Here we reproduce the water distributions similar to those in sandstones or glass assemblies by changing the values of  $I_i^{l,l}:I_i^{l,s}$  ratio, as shown in Figs. 11c and 11d. Now Fig. 11 compares the water distributions in the porous media for different phase interaction growth probabilities. The solid phase distributions are isotropic with the volume fraction  $\varepsilon = 0.5$  and the core distribution probability  $c_d = 0.01\varepsilon$ . The water volume fraction is 0.25 and the  $I_i^{l,l}:I_i^{l,s}$  ratio changes from 10:1 to 1:100. A greater value of the  $I_i^{l,l}:I_i^{l,s}$  ratio means a weaker liquid–solid interphase attractive potential and a weaker wetting interface, i.e., the liquid will be more aggregative as a result.

The phase interaction growth probability effects on the ETC of multi-phase porous media are thus studied. Assuming an unsaturated sandstone case where the solid particle volume fraction is  $\varepsilon = 0.5$  with  $c_d = 0.01\varepsilon$ , the water volume fraction is  $P_l = 0.3$ , and the component thermal conductivities are  $k_s = 3.0$  W/m K,  $k_l = 0.1$  W/m K, and  $k_g = 0.025$  W/m K, respectively. Fig. 12 shows the predicted ETC for different liquid–solid phase interaction growth probabilities. The results indicate that the ETC of multi-phase porous media increases with the degree of liquid phase conglomeration. The calculated ETC

changes little when the  $I_i^{l,l}:I_i^{l,s}$  ratio is less than 1, and increases remarkably when the  $I_i^{l,l}:I_i^{l,s}$  ratio is greater than 10.

## 5. Conclusions

To model and analyze the phase distribution effects on the effective thermal conductivity of multi-phase porous media, we have developed the quartet structure generation set (QSGS) for generating different kinds of multi-phase granular porous structures and the lattice Boltzmann method (LBM) for solving the energy transport equations efficiently with multi-phase conjugate effects considered. The numerical algorithms have been validated by a series of comparisons with existing theoretical solutions and experimental data.

The phase distribution characteristics were controlled by the parameters of QSGS and the effective thermal conductivities for various distributed porous media were then calculated by the LBM. The results showed that a smaller average particle size could lead to a better uniformity of phase distribution and a larger surface-to-volume ratio, both of which would result in a more uniform temperature gradient field for same temperature differences. Therefore the smaller is the average particle size, the larger is the effective thermal conductivity for a certain porosity, which agrees with the existing experimental phe-



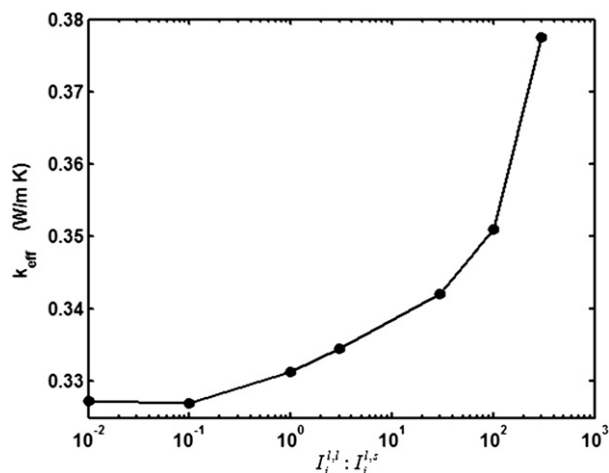


Fig. 12. ETC of three-phase porous media for different liquid–solid phase interaction growth probabilities. The parameters are:  $\varepsilon = 0.5$ ,  $c_d = 0.01\varepsilon$ ,  $P_l = 0.3$ ,  $k_s = 3.0$  W/m K,  $k_l = 0.1$  W/m K, and  $k_g = 0.025$  W/m K.

nomena. The anisotropy of porous media is controlled by the directional growth probability. If the larger directional growth probability is along the direction of temperature gradient, the ETC in this direction will be enhanced. As a result, the ETC in the vertical direction will be weakened. For three or more phase porous media, the degree of phase conglomeration is determined by the phase interactions, such as wetting properties. A larger liquid–liquid interaction leads to a higher degree of liquid phase conglomeration. The numerical results showed that the ETC of multi-phase porous media increases with the degree of liquid phase conglomeration.

## Acknowledgments

The present work is supported by a Grant from the NTC-M04-CD01 and NSF-061308 of USA and the NSF (59995550-2) of China.

## References

- [1] R.W. Zimmerman, J. Pet. Sci. Eng. 3 (1989) 219–227.
- [2] R.W. Zimmerman, Compressibility of Sandstones, Elsevier, New York, 1991.
- [3] M. Quintard, M. Todorović, Heat and Mass Transfer in Porous Media, Elsevier, New York, 1992.
- [4] A. Verruijt, Computational Geomechanics, Kluwer Academic, Boston, 1995.
- [5] D.B. Ingham, A. Bejan, E. Mamut, I. Pop, Emerging Technologies and Techniques in Porous Media, Kluwer Academic, London, 2003.
- [6] G.Q. Lu, X.S. Zhao, Nanoporous Materials—Science and Engineering, Chemical Engineering Series, Imperial College Press, London, 2004.
- [7] D.B. Ingham, I. Pop, Transport Phenomena in Porous Media III, Elsevier, Oxford, UK, 2005.
- [8] A. Sayari, M. Jaroniec, Nanoporous Materials IV, Elsevier, New York, 2005.
- [9] A. Bouguera, J. Phys. D Appl. Phys. 32 (1999) 1407–1414.
- [10] X.G. Liang, W. Qu, Int. J. Heat Mass Trans. 42 (10) (1999) 1885–1893.
- [11] J.E.J. Staggs, Fire Safety J. 37 (1) (2002) 107–119.
- [12] J.F. Wang, J.K. Carson, M.F. North, D.J. Cleland, Int. J. Heat Mass Trans. 49 (2006) 3075–3083.

- [13] L. Tacher, P. Perrochet, A. Parriaux, Transport Porous Med. 26 (1) (1997) 99–107.
- [14] M. Pilotti, Transport Porous Med. 33 (3) (1998) 257–278.
- [15] K. Makrodimitris, G.K. Papadopoulos, C. Philippopoulos, D.N. Theodorou, J. Chem. Phys. 117 (2002) 5876–5884.
- [16] D.S. Li, G. Saheli, M. Khaleel, H. Garmestani, Comput. Mat. Sci. 38 (1) (2006) 45–50.
- [17] N. Losic, J.F. Thovert, P.M. Adler, J. Colloid Interface Sci. 186 (1997) 420–433.
- [18] S. Torquato, Random Heterogeneous Materials: Microstructure and Macroscopic Properties, Springer-Verlag, New York, 2002.
- [19] S. Torquato, Int. J. Solids Struct. 37 (2000) 411–422.
- [20] S. Mohanty, J. Phys. D Appl. Phys. 30 (1997) L80–L84.
- [21] M. Wang, J.K. Wang, N. Pan, S.Y. Chen, Phys. Rev. E 75 (2007) 036702.
- [22] M. Wang, J.K. Wang, N. Pan, S.Y. Chen, J.H. He, J. Phys. D Appl. Phys. 40 (2007) 260–265.
- [23] P. Meakin, Fractals, Scaling and Growth Far from Equilibrium, Cambridge Univ. Press, 1998.
- [24] J.F. Thovert, F. Wary, P.M. Adler, J. Appl. Phys. 68 (1990) 3872–3883.
- [25] D. Coelho, J.F. Thovert, P.M. Adler, Phys. Rev. E 55 (2) (1997) 1959–1978.
- [26] K. Bakker, Int. J. Heat Mass Transfer 40 (15) (1997) 3503–3511.
- [27] A.G. Fedorov, R. Viskanta, Int. J. Heat Mass Transfer 43 (2000) 399–415.
- [28] A. Horvat, I. Catton, Int. J. Heat Mass Transfer 46 (2003) 2155–2168.
- [29] D.X. Zhang, Stochastic Method for Flow in Porous Media, Academic Press, London, 2002.
- [30] D. Kulasiri, W. Verwoerd, Stochastic Dynamics Modeling Solute Transport in Porous Media, Elsevier, New York, 2002.
- [31] Y. Shoshany, D. Prialnik, M. Podolak, Icarus 157 (1) (2002) 219–227.
- [32] S. Barta, P. Dieska, Kovove Mater. 40 (2) (2002) 99–112.
- [33] H.F. Zhang, X.S. Ge, H. Ye, Modell. Simul. Mater. Sci. Eng. 13 (3) (2005) 401–412.
- [34] H.F. Zhang, X.S. Ge, H. Ye, J. Phys. D Appl. Phys. 39 (1) (2006) 220–226.
- [35] J.Y. Qian, Q. Li, K. Yu, Y.M. Xuan, Sci. China Ser. E 47 (2004) 716–724.
- [36] X. Chen, P. Han, Int. J. Heat Fluid Flow 21 (2000) 463–467.
- [37] J.K. Wang, M. Wang, Z.X. Li, Int. J. Therm. Sci. 46 (3) (2007) 228–234.
- [38] X. He, L.S. Luo, Phys. Rev. E 55 (1997) 6333–6336.
- [39] T. Abe, J. Comp. Phys. 131 (1997) 241–246.
- [40] S.Y. Chen, G.D. Doolen, Annu. Rev. Fluid Mech. 30 (1998) 329–364.
- [41] D. Raabe, Modell. Simul. Mater. Sci. Eng. 12 (2004) R13–R46.
- [42] J.K. Wang, M. Wang, Z.X. Li, J. Colloid Interface Sci. 296 (2006) 729–736.
- [43] M. Wang, J.K. Wang, Z.X. Li, J. Colloid Interface Sci. 300 (1) (2006) 446.
- [44] Q.J. Kang, D.X. Zhang, S.Y. Chen, J. Geophys. Res. 108 (2003) 2505.
- [45] Q.J. Kang, D.X. Zhang, P.C. Lichtner, I.N. Tsimpanogiannis, Geophys. Res. Lett. 31 (2004) L21604.
- [46] M. Wang, J.K. Wang, S.Y. Chen, N. Pan, J. Colloid Interface Sci. 304 (1) (2006) 246–253.
- [47] S. Succi, The Lattice Boltzmann Equation for Fluid Dynamics and Beyond, Oxford Science Press, London, 2001.
- [48] X.Y. He, S.Y. Chen, G.D. Doolen, J. Comput. Phys. 146 (1998) 282–300.
- [49] Y. Peng, C. Shu, Y.T. Chew, Phys. Rev. E 68 (2003) 026701.
- [50] Q.S. Zou, X.Y. He, Phys. Fluids 9 (6) (1997) 1591–1598.
- [51] H.J. Lee, R.E. Taylor, J. Appl. Phys. 47 (1) (1976) 148–151.
- [52] A.R. Sepaskhah, L. Boersma, Soil Sci. Soc. Am. J. 43 (3) (1979) 439–444.
- [53] A.K. Singh, R. Singh, D.R. Chaudhary, J. Phys. D Appl. Phys. 23 (6) (1990) 698–702.
- [54] S. Fukusako, Int. J. Thermophys. 11 (2) (1990) 353–372.
- [55] G.N. Dulnev, D.P. Volkov, A.B. Utkin, J. Eng. Phys. Thermophys. 52 (2) (1987) 213–217.
- [56] V.V. Polyakov, M.A. Utemesov, A.V. Egorov, J. Eng. Phys. Thermophys. 68 (5) (1995) 580–583.
- [57] K. Midttomme, E. Roaldset, Pet. Geosci. 4 (2) (1998) 165–172.
- [58] J.Z. Liang, F.H. Li, Polym. Test. 25 (4) (2006) 527–531.
- [59] X.G. Cheng, Z.X. Li, Z.Y. Guo, Sci. China Ser. E 46 (3) (2003) 296–302.
- [60] S. Torquato, Annu. Rev. Mater. Res. 32 (2002) 77–111.